

The stellar masses of 25000 galaxies at $0.2 \leq z \leq 1.0$ estimated by the COMBO-17 survey

Andrea Borch^{1,5}, Klaus Meisenheimer¹, Eric F. Bell¹, Hans-Walter Rix¹, Christian Wolf², Simon Dye³,
Martina Kleinheinrich¹, Zoltan Kovacs¹, and Lutz Wisotzki⁴

¹ Max-Planck-Institut für Astronomie, Königstuhl 17, D-69117 Heidelberg, Germany

² Department of Physics, University of Oxford, Denys Wilkinson Building, Keble Road, Oxford OX1 3RH, U.K.

³ School of Physics and Astronomy, Cardiff University, 5 The Parade, Cardiff CF24 3YB, U.K.

⁴ Astrophysikalisches Institut Potsdam, An der Sternwarte 16, D-14482 Potsdam, Germany

⁵ Astronomisches Rechen-Institut, Mönchhofstr. 12-14, D-69120 Heidelberg, Germany

Received 19 October 2005 / Accepted 25 March 2006

Abstract. We present an analysis of stellar mass estimates for a sample of 25000 galaxies from the COMBO-17 survey over the interval $0.2 < z < 1.0$. We have developed, implemented, and tested a new method of estimating stellar mass-to-light ratios, which relies on redshift and spectral energy distribution (SED) classification from 5 broadband and 12 medium band filters. We find that the majority ($> 60\%$) of massive galaxies with $M_* > 10^{11} M_\odot$ at all $z < 1$ are non-star-forming; blue star-forming galaxies dominate at lower masses. We have used these mass estimates to explore the evolution of the stellar mass function since $z = 1$. We find that the total stellar mass density of the universe has roughly doubled since $z \sim 1$. Our measurements are consistent with other measurements of the growth of stellar mass with cosmic time and with estimates of the time evolution of the cosmic star formation rate. Intriguingly, the integrated stellar mass of blue galaxies with young stars has not significantly changed since $z \sim 1$, even though these galaxies host the majority of the star formation: instead, the growth of the total stellar mass density is dominated by the growth of the total mass in the largely passive galaxies on the red sequence.

Key words. Galaxies: mass function – Galaxies: evolution

1. Introduction

Current models for the formation and evolution of cosmic structure and galaxies provide us with a picture of hierarchical structure formation, where large objects are built-up successively from the merging of smaller, previously formed objects (e.g. Blumenthal et al 1984; Davis et al. 1985) and from the more gradual inflow of gas (e.g. White and Rees, 1978; Murali et al. 2002). The dynamical aspects of CDM-based galaxy formation can by now be well described either by numerical ab-initio simulations (e.g. Springel & Hernquist 2003; Weinberg et al. 2004) or by semi-analytic modeling (Kauffmann et al. 1993; Cole et al. 1994; Cole et al. 2000; Somerville et al. 2001). Yet, when, how and how efficiently stars formed in the course of this evolution appears to depend sensitively on regulating feed-back and on sub-grid (i.e. unresolved) physical processes; consequently, the current generation of models has limited power to robustly address this most central question of galaxy formation.

In this context, an empirical assessment of the build-up of stellar mass from early epochs to the present is an important constraint. To explore the efficiency of star-formation and feed-back on different mass scales, one needs to derive not only the integrated stellar mass density $\langle \rho_* \rangle(z)$ as a function of epoch, but also the evolution of the stellar *mass function* of galaxies. At the present day, it has become clear that stellar mass correlates strongly with a broad range of galaxy properties, such as mass density, mean stellar population age, metallicity, or alpha enhancement (e.g., Bender, Burstein & Faber 1993; Kauffmann et al. 2003; Tremonti et al. 2004; Thomas et al. 2005). Study of how some of these scaling relations evolve with redshift will give still keener insight into star formation, feedback, and galaxy assembly through merging.

Over the last decade (e.g., Lilly et al. 1996; Madau et al. 1996) the global build-up of stellar mass has been traced by estimating the mean star-formation rate (SFR) as a function of cosmic epoch, $\langle \text{SFR}(z) \rangle$. These estimates have been based on either the UV luminosity (e.g. Steidel et al. 1999; Giavalisco et al. 2004, Schiminovich et al. 2005), on the resulting emission line excitation (e.g. Yan et al. 1999; Hippelein et al. 2003; Brinchmann et al. 2004)

Send offprint requests to: K. Meisenheimer, e-mail: meisenheimer@mpia.de

or on thermal infrared or radio emission (e.g., Flores et al. 1999; Haarsma et al. 2000; Le Floch et al. 2005). The UV- and line emission-derived estimates require large and uncertain dust extinction corrections (e.g., Meurer et al. 1999; Adelberger and Steidel 2000); thermal infrared and radio emission are less dust-sensitive but are currently limited in sensitivity to probing intensely star-forming galaxies at intermediate and high redshift. The latter approach therefore requires large corrections for the faint end of the IR or radio luminosity function to estimate $\langle \text{SFR}(z) \rangle$. Both approaches rely quite sensitively on a prior assumption for the stellar initial mass function, as the bolometric luminosity is dominated by the UV radiation from $\sim 5M_{\odot}$ stars, while the mass budget is made up by stars of solar mass and below. Finally, even perfect knowledge of the star formation density function at different redshifts, $\rho(\text{SFR}, z)$, does not contain enough information to predict the observable stellar mass function of galaxies, $p(M_*, z)$.

A conceptually obvious, but practically quite difficult, path to bypass these problems in estimating the build-up of stellar mass, is to estimate $p(M_*, z)$ directly from stellar mass measurements at different redshifts. Two observational avenues present themselves, dynamical mass estimates from kinematic measurements at different redshifts, and estimates of the stellar mass-to-light ratio (M/L) based on the spectral energy distribution (SED) of a stellar population. Dynamical mass estimates from molecular gas kinematics have now been demonstrated to redshifts $z > 2$ (e.g. Neri et al. 2003), but will remain restricted in the immediate future to exploring the relatively small fraction of massive, gas-rich galaxies. Kinematics of galaxies to $z \geq 1$ are now routinely being measured, both from absorption lines (e.g., Holden et al. 2005; van der Wel et al. 2005) and emission line rotation curves (Vogt et al. 1996, 1997; Böhm et al. 2004; Conselice et al. 2005); current published sample sizes are in the 10s to 100s.

Stellar luminosity is the simplest observational proxy for stellar mass, but cannot offer stellar masses with relevant precisions (better than about a factor of two), as the rest-frame optical M/L values of stellar populations with different SFHs can vary by more than an order of magnitude. Rest-frame near-infrared M/L ratios vary less as a function of star formation history; nevertheless, different plausible star formation histories differ still substantially in their rest-frame infrared M/L (by a factor of four or more).

However, the luminous properties of galaxies can be used to estimate stellar masses. Low-resolution ($R \sim 3 - 30$) galaxy spectral energy distributions (SEDs) do not contain enough information to robustly infer the SFH, metallicity, or dust content of a galaxy. Older stellar ages, higher metallicity, or more dust extinction all make SEDs redder. Yet, all these effects not only redden the SED, but also lower the emergent optical flux (at a given mass) by similar amounts. Hence, stellar M/L can be estimated from SED-template fits, the strength of the 4000Å- break (D4000) or even the $(B-V)_{\text{rest}}$ color, for a wide range of the above parameters (e.g., Brinchmann & Ellis 2000; Bell

& de Jong 2001; Papovich et al. 2001; Kauffmann et al. 2003). If spectra are available, this approach can be refined to include two or more spectral diagnostics, e.g. D4000 and $\text{EW}(\text{H}\delta)$ (Kauffmann et al 2003); indeed, recent works make use of higher-resolution spectra to robustly estimate stellar mass (e.g., Panter et al. 2004). Stellar masses estimated in these ways are consistent at the ~ 0.1 dex level (e.g., Bell et al. 2003; Drory et al. 2004b; Salim et al. 2005) and correlate strongly with dynamically-measured masses (e.g., Bell & de Jong 2001; Drory et al. 2004a; van der Wel et al. 2005; Cappellari et al. 2005). One has to be aware, however, that very dusty galaxies or galaxies with SFHs featuring by large and recent (less than 2 Gyr ago) bursts of star formation will have poorly-measured masses ($\gtrsim 0.3$ dex error) if not derived from template spectra accounting explicitly for these effects.

SED or spectra-based M/L estimates have been used to describe the local galaxy population (Cole et al. 2001; Bell et al. 2003; Kauffmann et al. 2003), based on samples of many thousands of galaxies, and on modest samples of distant galaxies $z \geq 1$, where deep near-IR data have permitted measurement of the optical rest-frame SEDs (e.g. Papovich et al. 2001, Rudnick et al. 2003, Drory et al. 2004a, 2005; Fontana et al. 2004). Studies of distant $z \geq 0.5$ samples have been hampered by a number of largely inevitable difficulties: small number statistics for the most massive galaxies, field-to-field variations (as quantified elegantly by Drory et al. 2004a and Somerville et al. 2004), and increased stellar mass uncertainties due to limited spectral coverage and/or the use of photometric redshifts.

The purpose of the present paper is to derive SED-based stellar mass estimates for all galaxies in the COMBO-17 sample (Wolf et al. 2001, 2003). We quantify field-to-field, number statistics, and photometric redshift uncertainties as carefully as possible. We then use those mass estimates for a comprehensive estimate of the global stellar mass density in the redshift range $1 > z > 0.2$, as well as of the galaxy mass function over the same period. This paper is organized as follows. Section 2 briefly recapitulates the data base of the COMBO-17 survey and outlines its redshift and SED determination. Section 3 describes the methodology for estimating galaxy masses and discusses the errors involved. Section 4 presents our results on the evolution of the stellar mass in galaxies since $z = 1$. In Section 5 we discuss these results in respect to previous work, the cosmic star formation history and models of galaxy formation. We assume $H_0 = 70 h_{70} \text{ km s}^{-1} \text{ Mpc}^{-1}$; $\Omega_{\Lambda} = 0.7$ and $\Omega_{\text{m}} = 0.3$ and adopt $h_{70} \equiv 1$.

2. The galaxy sample

Our analysis is based on the optical multi-color images in three fields (CDFs, Abell 901, 11h field) of the COMBO-17 survey (Wolf et al. 2003). We use the photometric catalog of Wolf et al. (2003), in the revised version presented by Wolf et al. (2004) to which we refer for further details. Each square field covers $\sim 950 \square'$ on the sky, correspond-

ing to a co-moving transverse size of ~ 22 Mpc at $z \sim 0.7$. The three fields are so widely separated as to be completely uncorrelated. The combination of deep observations in 5 broad bands (UBVRI) and 12 medium band filters between 400 and 930 nm, allows us to determine very accurate photometric redshifts (see Section 2.1, below and Wolf et al. 2004) and accurate UV–optical spectral energy distributions of galaxies (Section 2.2). Together, the three fields contain more than 26 000 galaxies with redshift estimates out to $z = 1.07$ which is the limit of reliable, precise redshift estimates based on optical filters only.

The multi-color photometry can be used to *a)* classify each object as star, galaxy, QSO or indeterminate, *b)* estimate its redshift, e.g. if it is a galaxy, and *c)* fit a template SED to the fluxpoints, and derive physical parameters, such as the stellar M/L . In principle, such a process can be carried out in one step (e.g., Rudnick et al. 2003) where classification, redshift and stellar mass are estimated jointly. However, experimentation with COMBO-17 data showed that physically-motivated template sequences with composite (old+young) stellar populations gave poorer redshift accuracy than the Wolf et al. (2004) dust-reddened single-burst template set. Consequently, in this paper we have adopted a two step classification process. First, we classify the objects and estimate redshifts using dust-reddened single burst templates (Wolf et al. 2004), which have been proven to give the best photometric redshifts as tested against a large spectroscopic training dataset, but clearly cannot provide the most realistic stellar masses. Therefore, the stellar masses of all galaxies and their uncertainties are obtained by fitting the optical 17-band SEDs with a new set of templates with more plausible SFHs.

2.1. Object classification and redshift estimates

In COMBO-17, objects are classified by their location in the 16-dimensional color space (Wolf et al. 2001). We use four broad-band color indices: $U - B$, $B - V$, $V - R$, $R - I$, and 12 medium band indices which always relate to the closest broad band filter. Color libraries of four object classes, namely main sequence stars, white dwarfs, galaxies and quasars, are used as templates. The galaxy templates span the redshift range $0 < z < 1.4$, the quasars the range $0 < z < 5$. In the first step, each object is assigned to one of these four types by comparing its observed colors (and their errors) to the color distribution of the templates. For an unambiguous classification, we require a relative probability of $p_i / \sum p_i \geq 0.75$. In fact, 98% of all objects at $R < 24$ are unequivocally assigned to one class by this requirement. The object classification relies primarily on colors; morphological information is used only for objects with $p_i / \sum p_i < 0.75$ for all classes.

For galaxies and quasars, we derive the joint probability of a given redshift and a given rest-frame spectral energy distribution (SED), accounting for photometric errors. The galaxy SEDs are represented by a set of simple

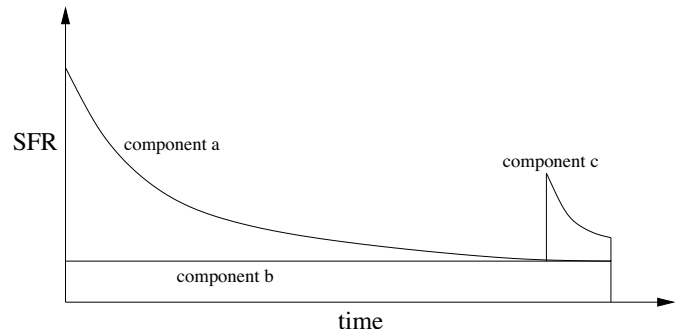


Fig. 1. Parameterization of the star formation history in our templates. An exponentially decaying star formation rate simulates an initial burst (component a). A second component b provides some constant star formation since the initial burst. For starburst galaxies a second burst in the recent past is assumed (component c).

templates (single-burst stellar populations with reddening) that was tuned to provide the most robust redshift estimates through comparison with spectroscopic redshifts (see Wolf et al. 2004). This procedure provides a *minimum error variance* estimation of both the redshift and the SED template. For this paper, galaxies with well-measured minimum-error-variance redshifts are used, with an additional R-band aperture magnitude cut $R_{\text{ap}} < 24$ to ensure that only galaxies with reasonably reliable redshifts are included in the analysis.

Wolf et al. (2004) have shown that in the redshift range $0.1 < z < 1.05$ the redshift accuracy of COMBO-17 is well approximated by

$$\sigma_z = 0.007(1+z)\sqrt{1+10^{0.8(R-21.6)}},$$

where R is the central R-band magnitude of the galaxy (measured in a $1''.5$ aperture), and does only weakly depend on galaxy color (SED).

2.2. Determining the SED of the galaxies

Obviously, the single burst templates used for the redshift estimates hardly can account for the wide variety of SFHs in galaxies. Detailed observations of resolved stellar populations (e.g., Rocha-Pinto et al. 2000; Harris & Zaritsky 2004) and integrated spectra (e.g., Trager et al. 2000; Proctor & Sansom 2002; Panter et al. 2004) show that most galaxies have formed stars over extended periods — oftentimes over almost a Hubble time. As old stars usually dominate the mass while young stars often dominate the optical flux, it is essential for estimating the mass-to-light ratio M/L to constrain their relative amount as accurately as possible from the observed SED.

Adopting the classification and redshifts from the simple templates, we estimate $(M/L)_*$ with a second SED template set that reflects more plausible SFHs. Specifically, we have devised a library of 100 spectral energy distributions built with the PEGASE-code (Fioc & Rocca-Volmerange 1997), sorted from red to blue

by an SED index S , $0 < S < 99$, which reproduces the sequence of mean UV-optical spectra of nearby galaxies collected by Kinney et al. (1996).¹ The underlying SFHs have been parameterized by the three-component model depicted in Figure 1. For the "old" population, we assume an exponentially decaying SFH (with e -folding time 1 Gyr) several billion years ago (component a), plus a constant star formation rate since the initial burst (component b). To reproduce the empirical SEDs between E galaxies and Sb galaxies in Kinney et al. (1996) we continuously decrease the age of initial burst by a factor of 2.5 and increase the b component to a maximum of $b/a = 0.16$ ². For even bluer galaxies (the "starburst galaxies" SB6 to SB1 in Kinney et al. (1996)) we include a second burst in the recent past (60 million years ago, component c). Its exponential decay time is kept constant, $\tau_c = 10^8$ yrs. Bluer galaxies are generated by increasing the relative amount of recent star formation c/a according to the prescription

$$c/a = 0.002 e^{S/17.2} - 0.021,$$

in the range $40 \leq S \leq 99$.

For component (a) we chose to follow the chemical evolution of the model galaxy using a closed box model, starting at 1/20 solar metallicity, as implemented in PEGASE. The metallicity of components (b) and (c) are chosen to be constant at solar metallicity. As we assume no infall and no galactic winds and start at 1/20 solar metallicity, our models will exhibit a significant G-dwarf problem. Furthermore, super-solar metallicities cannot be easily reached by this model; thus, the reddest SEDs (E, S0 type) can only be reproduced using unreasonably old ages of 20 Gyrs. Therefore, we regard the "ages" as meaningful only in a relative sense, with the age of the component a of the Sb galaxy found to be about $0.4 \times t_{max} = 8$ Gyr (where t_{max} refers to the age of the oldest stars in E/S0 galaxies)³. We have adopted a Kroupa IMF (Kroupa et al. 1993) and the mass regime $0.1-120 M_{\odot}$. The stellar M/L values and colors from such an IMF are very similar to those of a Kroupa (2001) IMF or a Chabrier (2003) IMF. Dust extinction is crudely accounted for using PEGASE (see Fiac & Rocca-Volmerange 1997 for details). In the code the dust optical depth is estimated from the gas mass

¹ In this way, the new library closely matches the template library which has been used in early implementations of the multi-color classification (see Wolf et al. 2001; 2003).

² Parameters a , b , and c are defined in terms of total stellar mass contained in each component; see, e.g., Equations 4 and 5.

³ It is important to note that, owing to the age/metallicity degeneracy for old stellar populations, the modest changes in stellar M/L caused by the old ages of the $S < 40$ templates are cancelled out by the substantially sub-solar metallicities of these templates. Thus, the template color–stellar M/L ratio correlation is in fact very similar to a solar metallicity, 7 Gyr old population for the $S < 40$ templates; such ages and metallicities are reasonably appropriate for modelling the $0.2 < z < 1.0$ galaxy population.

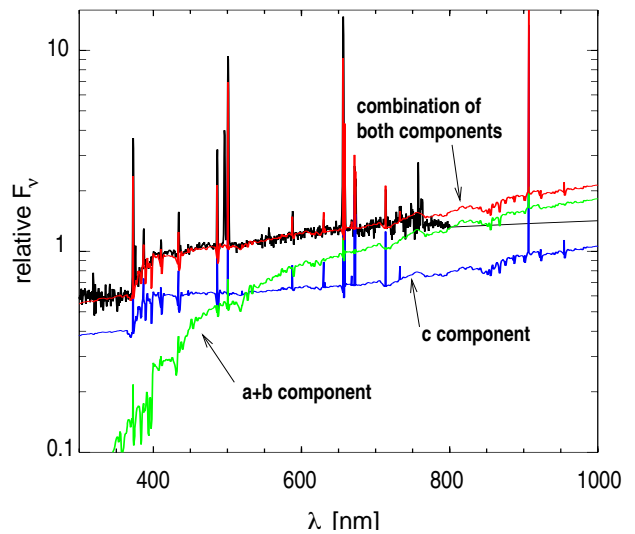


Fig. 2. An example for the template spectra for a starburst galaxy. The original Kinney et al. spectrum (SB-2) is shown and our best fit from the PEGASE spectra. It is composed of an old stellar population ($a + b$ component in Fig. 1) and a young stellar population (c component).

and metallicity, scattering is accounted for crudely following Calzetti et al. (1994). For component a we choose spheroidal geometry, while a plane-parallel slab geometry, averaged over all inclinations, is chosen for components b and c . This dust prescription reproduces many of the broad trends observed in local galaxies (e.g., Wang & Heckman 1996) reasonably well⁴.

In order to be suitable for multi-color classification, the one-dimensional library $S(0 \dots 99) = S(a, b, c)$ has to be monotonic both in color space and in the space of its astrophysical parameters: b/a , c/a and the age of the old stellar population. Figure 2 shows an example of one starburst galaxy from Kinney et al. (1996) and its composition from an old plus a young stellar population. For comparison with previous work we characterize the SED types S also by their rest-frame colors $U-V$ and $B-V$ (see Fig. 3).

The best-fitting SED is obtained by comparing the observed colors of each galaxy with the colors of the SED library spectra, shifted to the most likely redshift z as measured using the Wolf et al. (2004) classifier (Section 2.1).

3. Estimating stellar masses

Based on the $(M/L)_*$ of the best-fitting new SEDs, stellar masses can now be estimated. We choose to normalize the stellar mass by the reddest well-measured filter to minimize the influence of bursts of star formation. The medium-band filter which provides the best compromise

⁴ The color effects of age, metallicity and dust are largely degenerate when estimating stellar M/L from broad-band SEDs, therefore the detailed choice of this or a different dust model does not significantly affect our derived stellar masses.

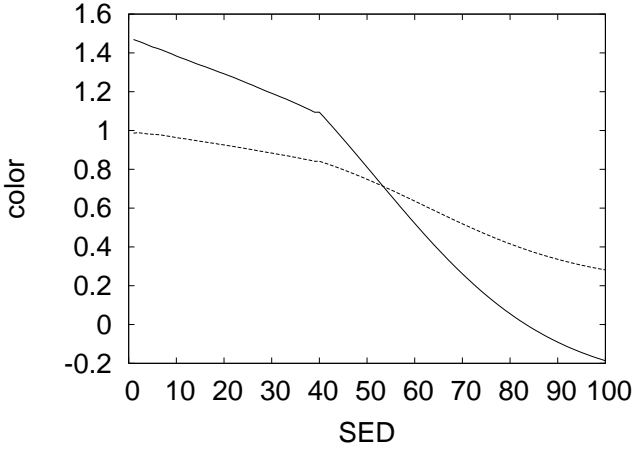


Fig. 3. Rest-frame colors U-V (solid line) and B-V (dotted line) as function of the SED type S in our library of galaxy templates.

between longest observed wavelength and signal-to-noise ratio is 816/21, with a central wavelength of 816 nm and a width of 21 nm. The 816/21 filter has a limiting magnitude of 22.9 (10σ) in all of our fields. The lower edge of the 816/21 filter, $\lambda_{\min} = 804$ nm, sets the maximum redshift where the stellar mass can be measured reliably: for a significant light contribution from the old stellar population, one needs to make sure that only flux at rest-frame wavelengths $\lambda_{\text{rest}} > 400$ nm is sampled. Hence, we restrict our current investigation to redshifts $z \leq 1.0$.

In practice, we convert the observed quantities z , S , f_{816} of each individual galaxy into stellar mass in the following way:

(1) The luminosity delivered from the PEGASE code, which is normalized to $1 M_{\odot}$, is used to calculate the apparent flux f_{λ} . For simplicity, we first consider only one component (luminosity F_{λ}). In this case the observed flux of a galaxy of stellar mass M is given by:

$$f_{\lambda} = \frac{\int F_{\lambda} \cdot Q_{\lambda} d\lambda}{\int Q_{\lambda} d\lambda} \cdot \frac{\frac{1}{m} \frac{M}{M_{\odot}}}{4\pi D_L^2(z)(1+z)/h_{70}^2}. \quad (1)$$

Here $m \cdot M_{\odot}$ denotes the *stellar* mass of the PEGASE template. The integral runs from 0 to ∞ . $Q_{\lambda} = q(\lambda)t(\lambda)$ is the spectral response of the system, in our case given by the transmission of the 816/21 filter and the quantum efficiency of the CCD. The factor $(1+z)$ accounts for the different wavelength scales of the observed flux f_{λ} and the rest-frame luminosity F_{λ} . Both F_{λ} and f_{λ} are given in $\text{W m}^{-2} \text{nm}^{-1}$.

In practice, COMBO-17 measures the central flux $f_{\gamma,ap}$ of each object in photon units $\gamma \text{m}^{-2} \text{s}^{-1} \text{nm}^{-1}$ (Wolf, PhD thesis) after convolving all images to a common effective PSF of 1.5 arcseconds. Thus, for well resolved galaxies, the central flux $f_{\gamma,ap}$ has to be corrected to the total flux $f_{\gamma,tot}$ by a correction factor η_{tot} . It is derived for each galaxy from the SExtractor MAG-BEST magnitudes (Kron magnitudes) on our very deep R-band image: $\eta_{tot} \equiv 10^{0.4(R_{ap}-R_{Kron})}$. Since we ignore wavelength

dependent aperture effects, the apparent flux f_{λ} in equ. (1) is approximated by:

$$f_{\lambda} = \frac{hc}{\lambda} f_{\gamma,tot} = \frac{hc}{\lambda} f_{\gamma,ap} \cdot \eta_{tot} \quad (2)$$

With equation (2), setting $f_{\gamma,ap} = f_{816}$, and solving formula (1) for the mass one gets:

$$\frac{1}{m} \frac{M}{M_{\odot}} = \frac{f_{816} \eta_{tot} \cdot 4\pi D_L^2(z) \cdot (1+z) \frac{hc}{\lambda} \int Q_{\lambda} d\lambda}{h_{70}^2 \cdot \int F_{\lambda} \cdot Q_{\lambda} d\lambda} \quad (3)$$

(2) As our templates are composed of three components a, b, c , both the luminosity and the stellar mass have to be synthesized: For each SED type $S_i = S(a, b, c)$ the total luminosity (per M_{\odot}) is

$$F_{\lambda} = a \cdot F_{\lambda,a} + b \cdot F_{\lambda,b} + c \cdot F_{\lambda,c}. \quad (4)$$

Similarly, the total stellar mass results from a linear combination of the individual components with the parameters a, b and c :

$$m = a \cdot m_a + b \cdot m_b + c \cdot m_c. \quad (5)$$

Here m_a, m_b and m_c are the *stellar* mass fractions of the respective components. Inserting (5) and (4) into equation (3), yields the final result:

$$h_{70}^2 \frac{M}{M_{\odot}} = \frac{f_{816} \eta_{tot} \cdot 4\pi D_L^2(z) \cdot (1+z) \frac{hc}{\lambda} \int Q_{\lambda} d\lambda}{\sum_{k=a,b,c} \frac{k}{m_k} \int F_{\lambda,k} \cdot Q_{\lambda} d\lambda}. \quad (6)$$

Equation (6) delivers the stellar mass of any galaxy with observed values f_{816}, η_{tot} , for which the classification has succeeded in determining the redshift z and the spectral type $S = S(a, b, c)$. The $< 2\%$ of galaxies for which no reliable redshift can be determined are faint and blue: misplacing them does only affect the mass function of blue galaxies below $3 \cdot 10^9 M_{\odot}$ (see Fig. 9).

3.1. Intrinsic errors

As obvious from equation (6), the intrinsic errors of the stellar masses depend both on the errors in redshift z (*via* $(1+z)D_L^2(z)$) and in SED type S (*i.e.* the M/L ratio: M/F_{λ}). Since a red SED at lower redshift can produce similar colors as a blue SED at slightly higher redshift, the errors in z and S are correlated. To account properly for this dependence we calculate the covariance matrix for each galaxy. To this end, besides determining the SED type $S(z_0)$ for the optimum redshift (according section 2.1, with its error σ_z), we let z vary in the interval $[z_0 - 2\sigma_z, z_0 + 2\sigma_z]$. From the corresponding points $S_i(z_i)$, we calculate the covariance matrix

$$C = \begin{pmatrix} P_i^2(\overline{(z_i - z_0)^2}) & P_i^2(\overline{(S_i - S(z_0))(z_i - z_0)}) \\ P_i^2(\overline{(z_i - z_0)(S_i - S(z_0))}) & P_i^2(\overline{(S_i - S(z_0))^2}) \end{pmatrix},$$

where each point is weighted by the probability

$$P_i = \exp \left[-\frac{1}{2} \left(\frac{z_i - z_0}{\sigma_z} \right)^2 \right]. \quad (7)$$

This matrix has to be diagonalized to obtain independent new parameters ζ and μ , calculated for each galaxy from the parameters z and S . The mass error is then estimated by gaussian error propagation from these new parameters and the error of the observed flux, σ_f :

$$\sigma_M = \sqrt{\left(\frac{\partial M}{\partial \zeta} \sigma_\zeta\right)^2 + \left(\frac{\partial M}{\partial \mu} \sigma_\mu\right)^2 + \left(\frac{\partial M}{\partial f_{\gamma,ap}} \sigma_f\right)^2}. \quad (8)$$

3.2. Calibration of mass scale and systematic errors

To investigate the global (average) properties of hundreds or thousands of galaxies within a redshift range, the statistical mass error of an individual galaxy is less important than any systematic error in the mass scale. We identify three main sources of systematic errors:

1. Overall calibration of the mass-to-light ratio scale.
2. SED dependent errors caused by an incorrect conversion from observed colors of a galaxy into an SED S (i.e. essentially: assuming an incorrect SFH which likewise fits the colors).
3. Redshift dependent errors, which could be either caused by sampling different rest-frame wavelengths or by using a common set of template spectra for a galaxy population which evolves with cosmic time.

In order to estimate how much these systematic effects might influence our results, we *first* compare (Fig. 4) the color- M/L relation from Bell et al. (2003) which is an update of Bell & de Jong (2001), scaled to a Kroupa et al. (1993) IMF, with the result of our mass estimation for all galaxies at $0.1 < z < 0.6$ (where the rest-frame V is sampled by the COMBO-17 photometry), and with R -band aperture magnitudes $R_{ap} < 23$ (to avoid excessive statistical errors). The discrepancies both at the blue and red end can be easily understood by the fact, that our template age-metallicity combination (red: metal poor and unreasonably old; blue: solar metallicity and young $\lesssim 0.1$ Gyr) should result in stellar M/L ratios at a given optical color which are very slightly smaller than those of Bell & de Jong (2001), who assumed 12 Gyr old populations and relatively high metallicities. Notwithstanding this slight difference, we conclude that the stellar M/L ratios used in this paper are very similar to those used for local studies, arguing that comparisons of this work to $z \sim 0$ studies should be reasonably robust.

Since our stellar masses are derived from observed-frame optical data alone, an independent *second* check of the robustness of the stellar mass estimates as a function of SED type is to compare the optical-only stellar masses with stellar masses derived from observed-frame near-infrared data. We have used deep, public, fully-reduced J , H , and K -band data on a 50 square arcminute sub-region of the CDFS taken with ISAAC at the VLT as a part of the ESO Imaging Survey EIS (Hatziminaoglou et al. 2002). Their limiting magnitudes are $J < 24.8$, $H < 23.4$ and

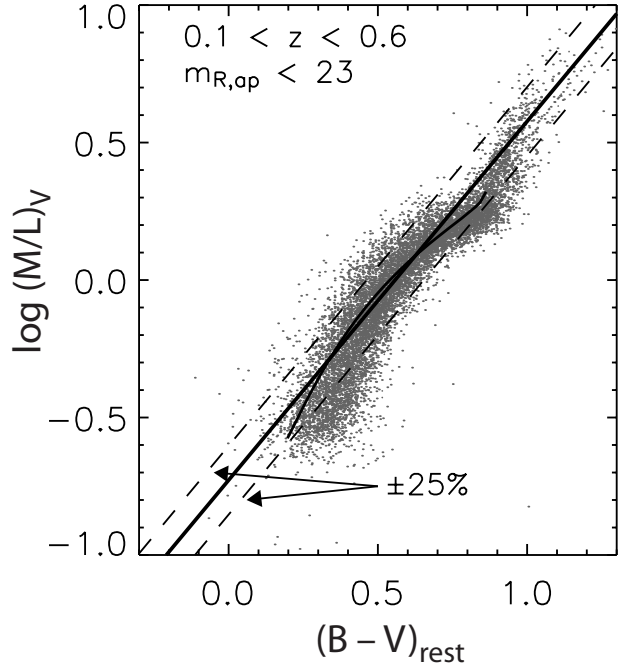


Fig. 4. V-Band mass to light ratio *versus* $(B-V)_{rest}$ color of COMBO-17 galaxies. For comparison the Bell et al. (2003) color- M/L correlation is shown as straight line. The transition between early type ($S < 40$) and blue galaxies occurs at $(B-V)_{rest} = 0.8$. Also overplotted is the color track of a sequence of exponential star formation histories with solar metallicity and age 7 Gyr (solid curve).

$K_s < 22.2$ (5σ , Vega system). Although this is only a small fraction of one COMBO-17 field, we find a sample of about 400 galaxies for which both a reliable COMBO-17 classification and near-infrared photometry are available.

We feed the ISAAC images directly in our COMBO-17 pipeline and re-calibrate the measured flux with respect to main sequence stars in the field.⁵ In order to allow matched photometry, the field distortions of the ISAAC camera have been corrected radially symmetrically, based on relative positions of bright objects on our deep R -band image and the individual J , H , K pointings.

For the comparison, we do not re-calculate best-fit redshifts and SED types using the optical and near-infrared data. Instead, we use the optically-derived redshifts and SED fits to blindly predict stellar M/L values for the observed-frame J , H , and K -bands, which are then multiplied by the J , H , and K -band photometry to derive new stellar masses⁶. That is, we do not attempt to find

⁵ This re-calibration accounts only for the global zero-point of the EIS data. From the main sequence stars we have some indications that the zero-points of the 8 subfields are slightly inconsistent with each other.

⁶ Recall that the default mass estimates were derived from SED-derived M/L s in the observed-frame 816/21 passband, multiplied by the 816/21 observed-frame luminosity.

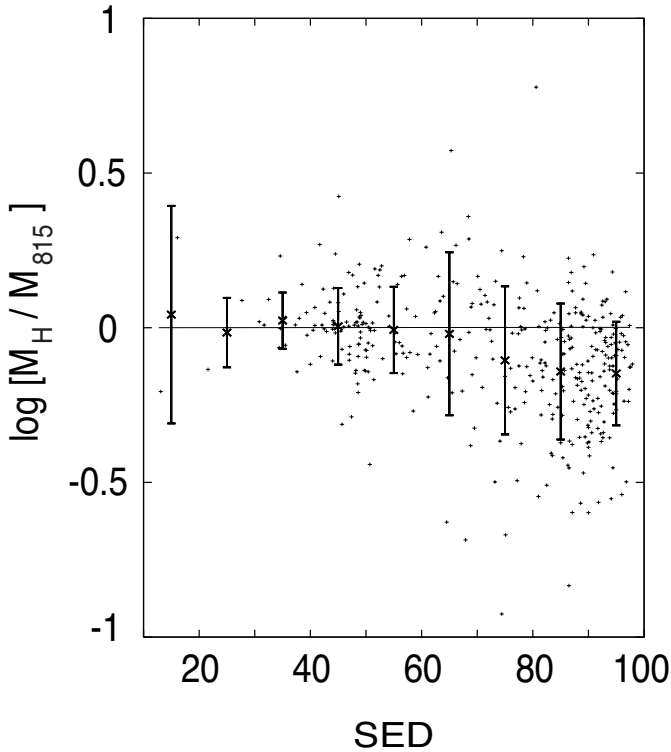


Fig. 5. Ratio between the stellar mass estimation based on the H -band and the stellar mass from the 816/21 filter as a function of SED type. The crosses with error bars show averages in SED bins ($\Delta S = 10$) and their rms variation.

a better overall solution for fitting the template spectra to *all* observed colors (16 optical plus 3 including the near-infrared). This approach has the advantage that we are sensitive only to the effect due to sampling different parts of the galaxy spectra for estimating the stellar mass. As the relative fraction of light from young and old stellar populations is a function of the rest-frame wavelength which is sampled, any inconsistencies between our synthesized spectra (and their composition) and the true spectra of the galaxies should become evident.

In Figure 5 the comparison between the mass estimations from filter 816/21 and from the H -band is shown as a function of SED type. The agreement is on average much better than 0.1 dex (25%) for early type and spiral galaxies ($S < 70$). Later templates — those with significant bursts of star formation in our template set with $S > 70$ — are offset by up to 0.15 dex in the sense that the optically-derived masses *overestimate* the stellar mass. The object-by-object scatter is largely accounted for by random errors in stellar mass: more than 60% of galaxies have mass differences of less than the combined mass uncertainties. The use of J -band for the mass derivation leads to similar results. If K -band is used for the mass derivation, again galaxies at $S < 70$ show consistent masses to within their combined uncertainties, whereas galaxies with the bluest

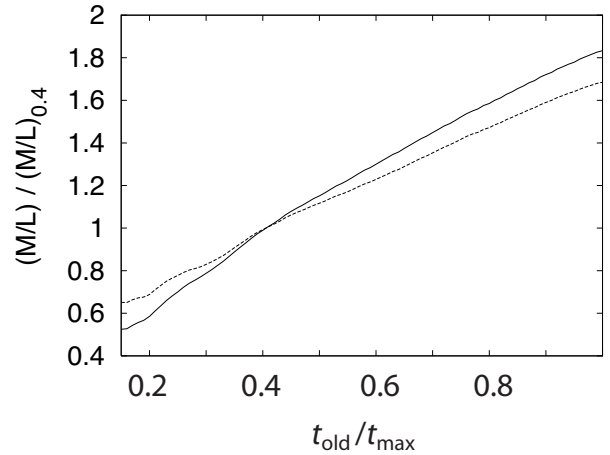


Fig. 6. Inferred stellar mass-to-light ratio for starburst galaxies as a function of the age of the underlying old stellar population (continuous line: V-band, dashed: K-band M/L). The plot shows the ratio between the true M/L ratio and that inferred with our $t_{old}/t_{max} = 0.4$ templates when classifying starburst galaxies for which we varied the age of the old stellar population. Note that both the V-band and K-band M/L ratio would be affected to a similar extent. The input template types were $50 < S < 90$.

stellar populations $S > 80$ show K -band derived stellar masses -0.3 dex lower than the optically-derived masses. While this offset is significant, it is worth bearing in mind that the masses of the bluest, most strongly star-forming galaxies were expected to be systematically uncertain at this level (owing to the unknown frequency of bursts of star formation; Bell & de Jong 2001; Kauffmann et al. 2003). Furthermore, galaxies with $S < 70$ — whose stellar masses appear to be consistently derived using either optical or near-infrared data — form more than 80% of the total integrated stellar mass at all $z < 1$. Thus, we conclude that the global results presented in this paper would not significantly change if near-infrared data were used in addition to the optical data to derive the stellar mass function evolution.

Although Bell & de Jong (2001) have demonstrated that there is an average correlation of the stellar M/L ratio and optical color for a wide variety of SFHs (see Fig. 4), different SFHs resulting in the same optical color might well differ by a factor of 2 in their M/L ratio. Our SED library has been constructed under the assumption that all blue galaxies ($S \geq 40$) possess a common old stellar population of age $t_{old} = 0.4 t_{max}$. Since at $z = 1$ the universe was half its present age, this assumption might introduce a redshift dependent systematic error in the mass of blue galaxies. As a *third* check we have investigated this effect by constructing blue galaxies with various values of t_{old} , subsequently classified with our template library (constant $t_{old} = 0.4 t_{max}$). As one can see from Fig. 6, increasing the age of the old stellar population by a factor of 2 (*i.e.* from

about 5 to 10 Gyrs) would increase the mass in blue galaxies by about 50%. On the other hand, assuming a much younger age, $t_{\text{old}} = 0.2t_{\text{max}}$ could lower the mass in blue galaxies by 40%. We conclude that this effect introduces a ~ 0.1 dex uncertainty in the evolution of stellar mass in blue galaxies in the 4 Gyr from $z = 0.9$ to $z = 0.3$ (the redshift range probed by our study), and a $\ll 0.1$ dex uncertainty in the evolution of total stellar mass over that period (as blue galaxies do not dominate the total stellar mass at any redshift).

4. Results

4.1. The relationship between color and stellar mass

Figure 7 shows the stellar mass estimates for the COMBO-17 galaxies as function of rest-frame U-V color. The solid black line indicates the (evolving) separation of ‘red sequence’ from ‘blue cloud’ galaxies, proposed by Bell et al. (2004), after conversion into the $M_* - (U - V)_{\text{rest}}$ plane:

$$(U - V)_{\text{rest}} > 0.227 \log_{10} M_* - 1.16 - 0.352z, \quad (9)$$

Not only locally ($z < 0.3$) but also at high redshift $z \simeq 1$ the intrinsically red (and for the most part old and non star forming) galaxies constitute over 60% of the very massive galaxies ($M_* > 10^{11} M_{\odot}$).

4.2. Completeness limits

It is obvious from Fig. 7 that the R-band flux limit of COMBO-17 leads to a mass cut (denoted roughly by the grey line in each panel of Fig. 7), which does not only depend on redshift but quite strongly on the rest-frame galaxy color: the least massive red galaxies contained in our sample typically have $10\times$ higher masses than the least massive blue galaxies. Thus, the strict mass completeness limit is set by the red sequence galaxies. We estimate an approximate completeness limit by selecting the mass value above which we find 80% of our detected red sequence galaxies in the respective redshift bin (vertical dotted lines in each redshift panel of Fig. 7). These strict limits are very conservative; in particular, the blue galaxy mass function will be complete well below this limit. The same limits, evaluated for the upper boundary of each redshift bin, are also shown in the mass function plots (see Figs. 8 & 9).

4.3. The evolution of the stellar mass function

We now use the estimated stellar masses of galaxies up to $z = 1.0$ to derive the evolution of the stellar mass function. Since our redshift slices are thin ($\Delta z = 0.2$) and the limiting mass is evaluated at the upper boundary of each bin, our samples are effectively volume limited down to that limiting mass and we do not use a V_{max} correction. We apply individually-derived completeness corrections to each detected galaxy (see, e.g., Wolf et al. 2003 for a full

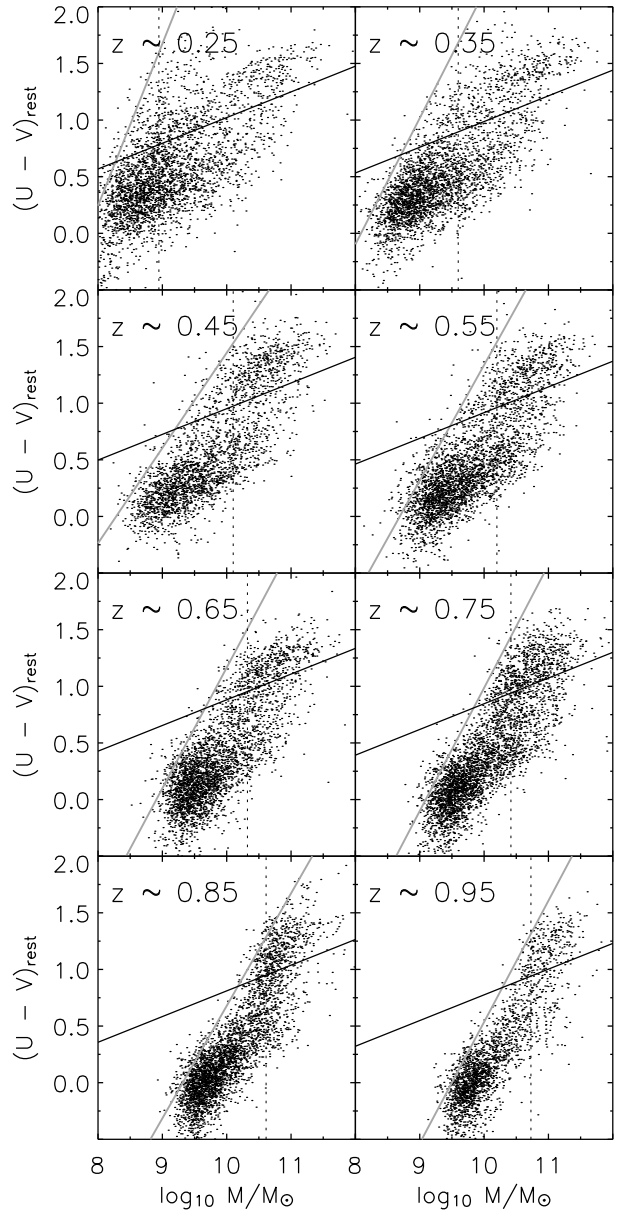


Fig. 7. Stellar mass *versus* rest-frame U-V color in different redshift bins. Middle redshift of the $\Delta z = 0.1$ wide bins is given in the upper left of each panel. The solid black line shows the separation between red sequence and blue cloud galaxies (equation (10)). The grey line indicates the approximate effect of the adopted apparent magnitude cut ($m_R < 24$) for successful redshift classification. The dotted lines indicate completeness limits for red sequence galaxies; blue cloud galaxies are complete well below this limit.

description of the completeness properties of COMBO-17). These were derived by putting artificial galaxies into COMBO-17 images and applying the COMBO-17 detection and classification pipeline. The completeness correction was derived as a function of $(z, m_{R,ap}, U - V)$ by con-

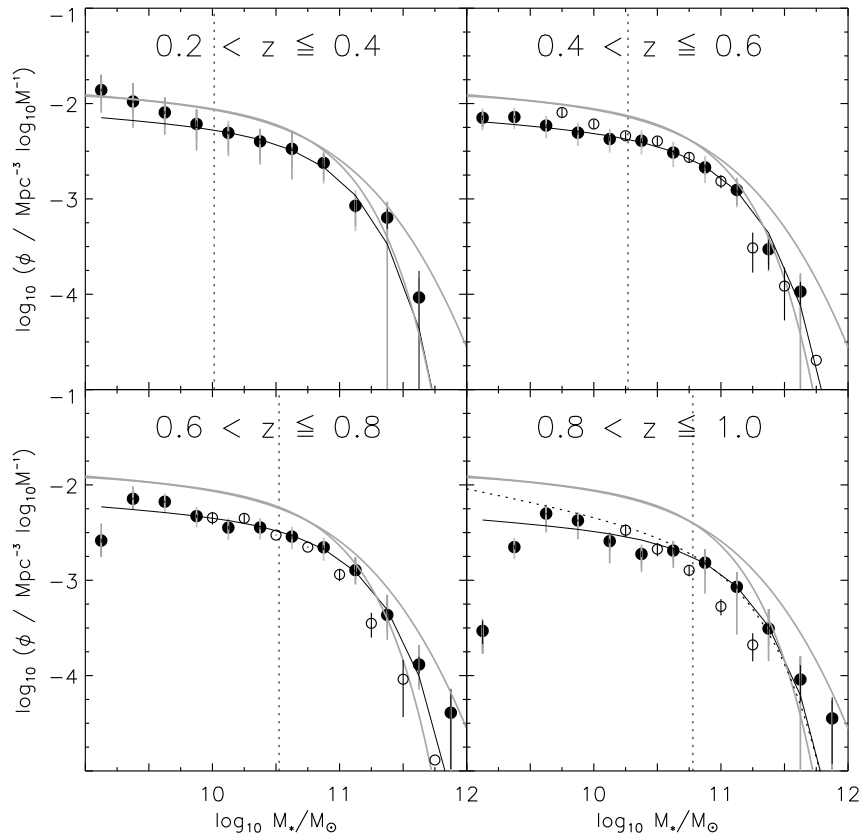


Fig. 8. Stellar mass function of all galaxies in different redshift bins (filled circles). The error bars account for Poisson uncertainties and cosmic variance as estimated from the full range of field-to-field variation (dark grey) and following Somerville et al. (2004; light grey). The solid line represents a Schechter function fit (with constant faint end slope α , assumed to be $\alpha = -1.1$ following the $z \simeq 0$ result of Bell et al. 2003). The lower grey line shows the local mass function; the upper grey curve shows the local mass function convolved with a log normal distribution of width 0.3 dex to simulate the effect of photometric redshift and stellar mass errors on the recovered mass function of high-mass galaxies. The vertical dotted line shows the completeness limit (for red galaxies) taken from Fig. 7. Open circles show comparison mass functions from Drory et al. (2004a), and the dotted line in the highest-redshift bin shows the Schechter fit to the stellar mass function from Fontana et al. (2004).

structuring the ratio of number of recovered galaxies to by the number of galaxies inserted into the same bin in redshift, R -band aperture magnitude and $U - V$ rest-frame color. That is, this completeness correction corrects the number of detected galaxies in a given bin in redshift, rest-frame colour and magnitude: in practice, this correction does not exceed 20% for objects classified as galaxies. It does not correct for galaxies not classified by COMBO-17, i.e. which are too faint to be classified or have highly unusual 17-passband SEDs.

The results are shown in Fig. 8 (total for all galaxies) and Fig. 9 (split into blue and red galaxies). The parameters of the Schechter fits (shown by the continuous and dotted lines in Figs. 8 & 9) are given in Table 1. Schechter functions are fit to galaxies only above our conservative completeness limit (as denoted by the dotted line). The data lack the depth to allow robust estimation of the faint end slope α . A number of strategies could have

been adopted; we chose to assume the same values of α as found locally: $\alpha = -1.1$ (all galaxies), $\alpha = -0.7$ (red galaxies), and $\alpha = -1.45$ (blue galaxies) following Bell et al. (2003)⁷. Mass function parameters for the local sample are reproduced in Table 1 converted to the cosmology adopted in this paper and using a universal Kroupa et al. (1993) IMF (for reference, stellar masses calculated with a Chabrier 2003 IMF would be similar to within a few percent).

Figure 8 shows clearly that the evolution of the *total* mass function is relatively modest. Since the low-mass end is completely dominated by blue galaxies (*c.f.* Fig. 9), for which the completeness reaches to smaller masses, the

⁷ Other strategies could have been adopted for constraining α , e.g., adopting the faint end slopes of the luminosity functions as derived by Willmer et al. (2005). We chose to adopt values of α fixed to locally-determined values to facilitate comparison of mass functions from $z = 1$ to $z = 0$.

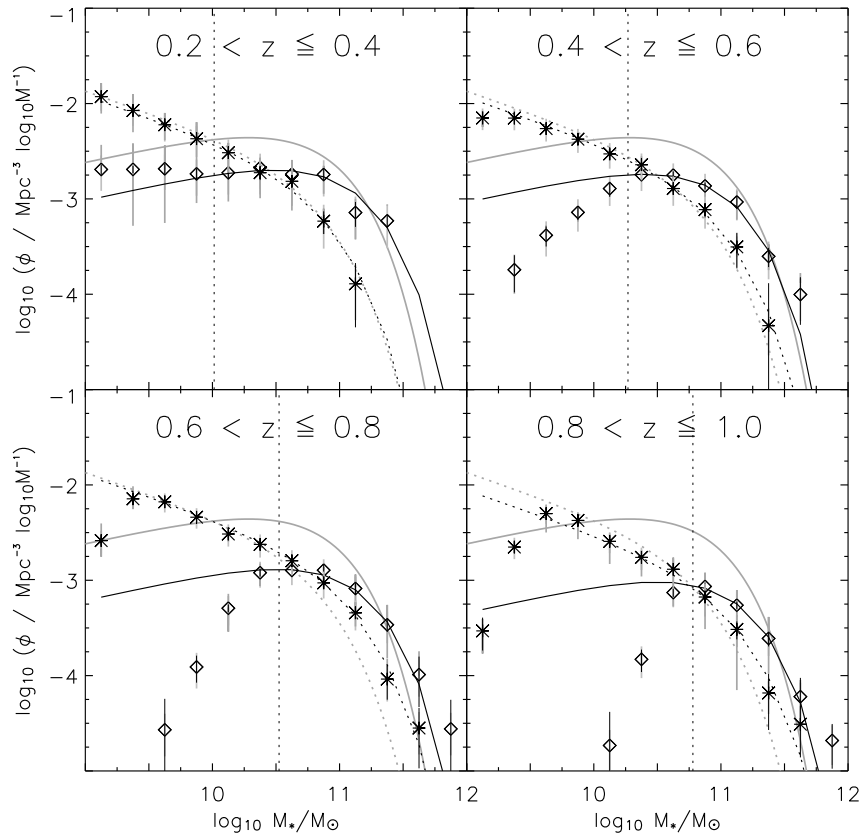


Fig. 9. Stellar mass function of *red* (\diamond) and *blue* ($*$) galaxies in different redshift bins. The solid black line represents a fit of the red galaxies with a Schechter function (with $\alpha = -0.7$). The Schechter fit to the blue galaxy stellar mass function is shown as dotted black curve (assuming $\alpha = -1.45$). The local mass functions, taken from Bell et al. (2003), are shown in grey. The error bars account for Poisson and field-to-field uncertainty. The vertical dotted line shows the completeness limit for red galaxies.

stellar mass function continues to rise well below the formal mass limit (recall, the mass limit is defined for red galaxies). We show also near-infrared derived stellar mass functions from MUNICS (Drory et al. 2004a; open circles) in the $0.4 < z \leq 0.6$, $0.6 < z \leq 0.8$, and $0.8 < z \leq 1.0$ bins, and the Schechter fit to the K20-derived mass function of Fontana et al. (2004) in the $0.8 < z \leq 1.0$ bin. Overall, the agreement between COMBO-17’s and other, near-infrared derived $z < 1$ stellar mass functions is excellent if one takes into account the large error bars at the bright end (due to small number statistics). In a recent study Bundy et al. (2006) present K-band based mass estimates of 8000 galaxies from the DEEP2 redshift survey (Davis et al. 2003). Although their split between red and blue galaxies, and redshift binning differ from ours, they find very similar results.

4.4. The evolution of the stellar mass function of red and blue galaxies

Owing to the COMBO-17’s number statistics and photometric redshift quality, it is possible not only to constrain

the total stellar mass function, but to also construct mass functions of the red sequence and blue cloud separately. The results are shown in Fig. 9. Diamonds and solid lines (black: fit to the data, gray: local color-split mass function) show the stellar mass function of red sequence galaxies. Asterisks and dotted lines show the stellar mass function of blue cloud galaxies. The vertical dotted line shows the position of the completeness limit for red-sequence galaxies: it is clear from the data points that red sequence galaxies become dramatically incomplete at low masses, whereas the mass function of blue galaxies continues to rise steeply.

Focusing on the blue cloud galaxies (asterisks and dotted lines), it is clear that there is relatively little change in their mass function since $z \sim 1$. In this framework, the observed rapid changes in L^* in the blue galaxy luminosity function (e.g., Lilly et al. 1995; Wolf et al. 2003; Willmer et al. 2005) have to be interpreted in terms of an unchanging characteristic stellar mass M^* and a rapidly evolving mean stellar M/L ratio (and therefore a rapidly evolving average color with redshift, as is indeed observed).

Table 1. Result of the Schechter fits to the mass function.

z	$\phi^* \times 10^4$	$\log_{10} M^*$	α	$\log_{10} \rho^*$
All galaxies				
0.0	35 ± 4	10.91 ± 0.10	-1.1 ± 0.02	8.48 ± 0.10
0.3	19 ± 9	11.03 ± 0.08	-1.1	8.34 ± 0.15
0.5	18 ± 6	11.02 ± 0.08	-1.1	8.32 ± 0.11
0.7	16 ± 5	11.09 ± 0.15	-1.1	8.33 ± 0.10
0.9	12 ± 4	11.08 ± 0.11	-1.1	8.17 ± 0.18
Red sequence				
0.0	37 ± 4	10.81 ± 0.10	-0.7 ± 0.07	8.33 ± 0.10
0.3	17 ± 7	10.97 ± 0.09	-0.7	8.17 ± 0.18
0.5	15 ± 5	10.95 ± 0.10	-0.7	8.08 ± 0.11
0.7	11 ± 4	11.06 ± 0.18	-0.7	8.05 ± 0.10
0.9	9 ± 3	11.01 ± 0.08	-0.7	7.89 ± 0.18
Blue cloud				
0.0	9.4 ± 1.0	10.80 ± 0.10	-1.45 ± 0.03	7.98 ± 0.10
0.3	7.5 ± 3.6	10.86 ± 0.19	-1.45	7.94 ± 0.15
0.5	7.2 ± 2.2	10.93 ± 0.12	-1.45	8.00 ± 0.11
0.7	6.4 ± 2.2	11.07 ± 0.07	-1.45	8.08 ± 0.10
0.9	5.3 ± 1.7	11.00 ± 0.25	-1.45	7.93 ± 0.10

Focusing instead on the red sequence (diamonds and solid lines), there is rapid evolution in their stellar mass function. Assuming a constant faint-end slope (which we cannot meaningfully constrain in this work⁸), the formal fits prefer evolution in ϕ^* (such that ϕ^* increases towards the present day) without significant change in M^* . It is worth noting that this result is insensitive to the detailed choice of color–mass cut used to separate the red and blue populations — as long as the cut is somewhere in the ‘gap’ between the red and blue populations.

4.5. The evolution of stellar mass densities

The average stellar mass density $\rho_* \equiv \int \Phi(m) dm$ is calculated by integrating the Schechter functions of Table 1 between $m = 0$ and ∞ . The mass density ρ_* for *all* galaxies is calculated for all three COMBO-17 fields; the larger of *i*) the field-to-field scatter, divided by $\sqrt{2}$, or *ii*) the predicted variance, following Somerville et al. (2004) given a number density and redshift, is adopted as the cosmic variance error bar. The results in Fig. 10 show, that the total stellar mass has increased substantially between $z \sim 1$ and the present day. Interestingly, much of the evidence for this growth comes from the comparison to the local stellar mass density⁹. Importantly, this stellar

⁸ Kodama et al. (2004) and de Lucia et al. (2004) present deeper data which show some evidence for a deficit of faint red-sequence galaxies at $z \sim 1$ compared to the present-day red-sequence galaxy stellar mass function.

⁹ In this context, it is worth noting that the local total stellar mass densities, and indeed those split by color, calculated by a variety of different groups are very similar with < 0.1 dex

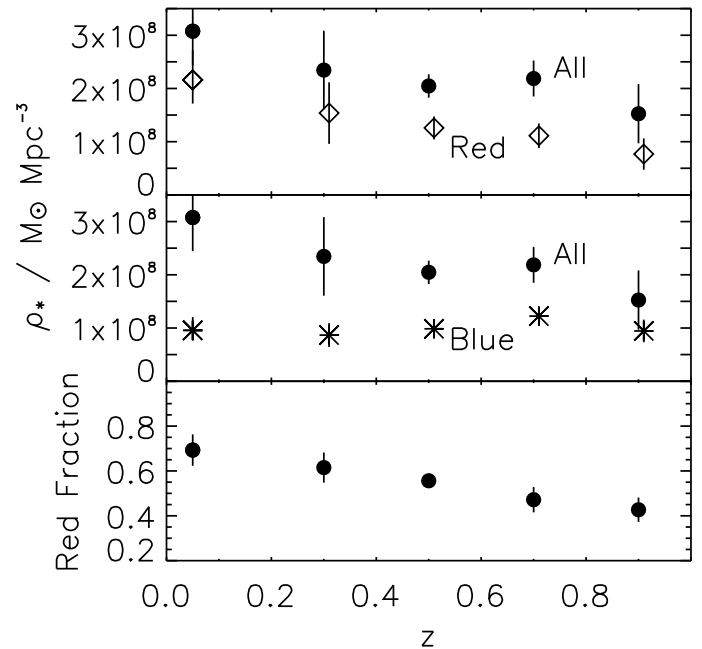


Fig. 10. The integrated stellar mass density as a function of redshift. In the upper two panels the total mass density for all galaxies (filled circles) is compared with those for red-sequence galaxies (diamonds), and for blue cloud galaxies (asterisks) separately. The lower panel shows the fraction of mass in red sequence galaxies as a function of redshift. In all cases, mass functions are integrated down to zero mass and error bars come from field-to-field variation divided by $\sqrt{2}$. The $z = 0$ datapoint is taken from Bell et al. (2003).

mass growth is dominated by the growth of the total stellar mass in red-sequence galaxies, while the total stellar mass in blue cloud galaxies is roughly constant over the last 8 Gyr.

5. Discussion

The COMBO-17 data and analysis constitute one of the first opportunities to combine large samples of galaxies to $z \sim 1$, rather precise redshifts (average $\sigma_z/(1+z) \simeq 0.02$), and accurate rest-frame colors $(U-V)_{\text{rest}}$ luminosities and stellar mass estimates. In particular, its rest-frame colors are accurate enough to allow for the first time the exploration of the mass growth of red and blue galaxies separately.

5.1. SED-based Stellar Mass Estimates

Through extensive SED matching, based on the PEGASE models (Fioc and Rocca-Volmerange 1997), we have illustrated scatter if IMFs and cosmologies are accounted for, giving confidence in the robustness of the locally-measured stellar mass density estimates (e.g., Cole et al. 2001; Kochanek et al. 2001; Bell et al. 2003; Baldry et al. 2004; Panter et al. 2004).

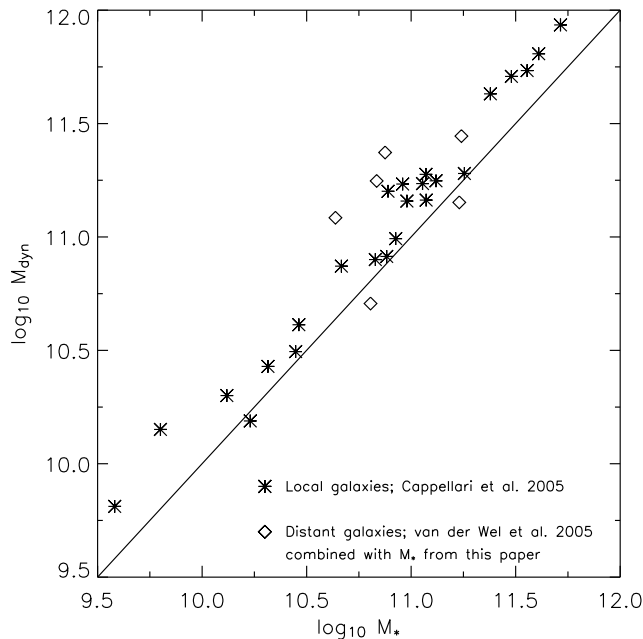


Fig. 11. A comparison of stellar and dynamical masses. Accurate stellar and dynamical masses (asterisks) are taken from Cappellari et al. (2005) for a sample of local early-type galaxies. Dynamical masses (van der Wel et al. 2005) for 6 COMBO-17 galaxies at $0.6 < z < 1.05$ with robust stellar masses are shown as diamonds.

trated the strength and limitations of stellar mass estimates based on this approach. We have shown that for a given IMF (e.g. Kroupa et al. 1993), the present modelling indicates that SED-based M/L estimates are better than a factor of two for most individual galaxies, with systematic sample uncertainties probably $< 30\%$ (c.f. Fig. 4 and Section 3.5, see also Drory et al. 2004b). We stress, however, that the masses derived here simply scale for different IMFs (below $2M_{\odot}$); e.g. for a Salpeter (1955) IMF all masses would be higher by a factor of 1.8.

Note that the analysis of the redshift dependence of stellar masses does not require an accurate absolute calibration of the stellar mass scale; rather, relative consistency between the stellar mass scale at $z \sim 1$ and $z \sim 0$ is sufficient. Figure 11 shows the comparison between a sample of local early-type galaxies with accurately-derived stellar and dynamical masses (Cappellari et al. 2005; a Kroupa 2001 IMF is adopted in that work, which has a very similar mass scale to the Kroupa et al. 1993 IMF) and a sample of 6 distant early-type galaxies in the Chandra Deep Field South with robust dynamical mass estimates from deep spectroscopy (van der Wel et al. 2005) and stellar mass estimates from this paper¹⁰. There is a clear

¹⁰ A substantial fraction of the van der Wel et al. sample were at or below the COMBO-17 $m_R < 24$ limit and had poorly-estimated or undefined redshift.

relationship between stellar and dynamical mass¹¹, and this relationship seems independent of redshift at least out to $z \sim 1$. This gives us some confidence that stellar population masses are being estimated consistently for local and distant samples, thus evolutionary trends between COMBO-17 and local samples should be relatively robust.

Our study illustrates quite dramatically how galaxy samples, even when selected at red observed bands, are very far from a stellar mass limited sample. The difference in stellar mass between the bluest and reddest galaxies at a given flux limit is a factor 8 at $z \simeq 0.3$ and more than 30 at $z \simeq 1$ (where the sample-selecting R-band corresponds to $\lambda_{\text{rest}} \sim 360$ nm).

5.2. The relationship between color and stellar mass

Our most conspicuous astrophysical result is that at $z < 1$, the majority of the most massive galaxies ($M_* > 10^{11}M_{\odot}$) are on the red sequence (see Figs. 7 and 9). This has qualitatively been clear from color–luminosity diagrams (e.g., Bell et al. 2004), but Figs. 7 and 9 demonstrate that it holds true for the top decade in stellar mass. It is not clear, at this stage, what this result implies in terms of galaxy evolution. The stellar mass functions (Fig. 9) show a very modest increase in the number of red massive ($M_* > 10^{11}M_{\odot}$) galaxies and a modest decrease in the number of blue massive ones from $z = 1$ to the present day. Yet, it is important to bear in mind that uncertainties in stellar masses and photometric redshifts have a particularly strong effect on the high-mass end of stellar mass functions; therefore, we argue that it is not clear whether the massive galaxy population was largely in place and non-star-forming at $z \sim 1$ (e.g. Saracco et al. 2005), or whether there has been some growth of massive non-star-forming galaxies through processes such as dry mergers (e.g. Bell et al. 2005b).

Over the last decade, there has been extensive evidence for what has become known as ‘downsizing’: while massive galaxies form stars at high redshift (e.g., Chapman et al. 2003; Daddi et al. 2005), only low-mass galaxies form significant numbers of stars at the present (Cowie et al. 1996; Heavens et al. 2004; Juneau et al. 2004; Bauer et al. 2005; Bell et al. 2005a; Tanaka et al. 2005; Kelm et al. 2005). The color-split mass functions presented in this paper allow us to explore some aspects of this effect. Figure 9, for instance, shows the evolution of the mass at which the red sequence (= non-star-forming) and blue cloud (= star forming) stellar mass functions cross¹² very similar to that adopted by Kauffmann et al. (2003), who explore the

¹¹ Note that dynamical mass should always be in excess of stellar mass (allowing the existence of dark matter in the inner parts of galaxies); clearly a Kroupa et al. (1993), Kroupa (2001) or Chabrier (2003) IMF satisfies these constraints whereas the Salpeter (1955) IMF (which produces stellar masses ~ 0.25 dex larger) would violate this constraint (see Cappellari et al. 2005; Bell & de Jong 2001).

¹² This definition is identical to Bundy et al.’s (2006) transition mass M_{tr} , and is

distribution of 4000 Å break strengths as a function of stellar mass.: above this mass the majority of galaxies is red and below it the majority of galaxies is blue. We find that this characteristic mass is $\sim 10^{10.8} M_{\odot}$ at $z = 1$ (in agreement with estimates presented in Bundy et al. 2006) and decreases by a factor of 5 or more to $\sim 10^{10} M_{\odot}$ at $z \simeq 0$. Yet, the physical significance of this ‘transition mass’ is not obvious as the stellar mass function of blue galaxies does not change significantly in the epoch $0 < z < 1$, suggesting that the maximum mass that galaxies reach while forming stars remains roughly the same. The apparent evolution of the ‘transition mass’ is driven entirely by the increasing prominence of the non-star-forming red sequence galaxies. This emphasizes the need for care when discussing ‘downsizing’, and the utility of large samples of galaxies with robust estimates of stellar masses for studying the physics driving the order-of-magnitude decrease in cosmic star formation rate since $z \sim 1$ (e.g., Le Floch et al. 2005).

5.3. The build-up of stellar mass

It is interesting to compare the COMBO-17-derived stellar mass density evolution since $z \sim 1$ with other work that has studied the build-up of the galaxy population since $z \sim 4$. The results are shown in Fig. 12. The top panel shows the total stellar mass in galaxies as a function of redshift (integrated to zero mass) for a variety of studies. The stellar masses have been adjusted to be consistent with a Kroupa et al. (1993), Kroupa (2001) or Chabrier (2003) IMF; all three IMFs have a stellar M/L at a given optical color that are 0.25 dex lower than for a Salpeter (1955) IMF, and all three IMFs are consistent with dynamical constraints (Bell & de Jong 2001; Cappellari et al. 2005), while a Salpeter IMF over-predicts the dynamical masses of many galaxies. Despite the inevitable uncertainties associated with estimating stellar masses, and cosmic variance, Fig. 12 illustrates that the different studies have come to a reasonably consistent picture of the growth of stellar mass with cosmic time.

This growth of stellar mass should be consistent with the integral of current measurements of the cosmic SFR. The lower panel of Fig. 12 shows the evolution of the cosmic SFR (adapted from Hopkins 2004). We have chosen not to convert the cosmic SFR measurements from a Salpeter (1955) IMF to a Kroupa et al. (1993) IMF in this work: as the power-law index of a Kroupa et al. (1993) IMF is substantially steeper than those of a Salpeter, Chabrier or Kroupa (2001) IMF for high-mass stars (which dominate the SFR measurements, but do not significantly affect broad-band SED-derived stellar masses), the use of a Kroupa et al. (1993) stellar IMF in what follows would lead to a factor of three over-production of stars. Instead, we adopt a Chabrier (2003) IMF (which has the same high-mass IMF slope as a Salpeter IMF and very similar stellar M/L s to a Kroupa et al. (1993) or Kroupa (2001) IMF), and ask the question whether the integral of the

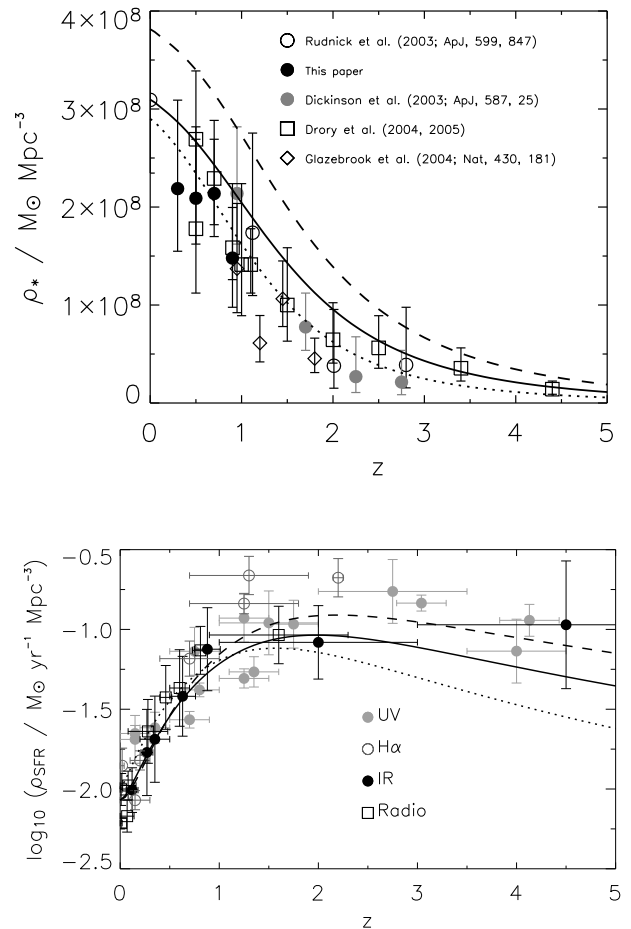


Fig. 12. Top: the growth of stellar mass density with cosmic time, as estimated from a number of surveys. Bottom: the evolution of the cosmic star formation rate, adapted from Hopkins (2004). In both panels, the stellar IMF has been adjusted to be consistent with Chabrier (2003); a Kroupa et al. (1993) IMF has a stellar M/L consistent with such an IMF but would produce star formation rates a factor of three higher than the Chabrier (2003) IMF. The lines show different assumptions for the evolution of the cosmic star formation history and the associated growth of cosmic stellar mass: the dotted line shows the fit optimized to reproduce the growth of stellar mass, the dashed line fits the star formation rate better, and the solid line is a reasonable compromise between the two.

cosmic star formation rate is consistent with the observed growth of stellar mass. We show three cosmic star formation histories and their integrals (accounting fully for gas recycling). The dashed line is a fit optimized to reproduce the evolution of cosmic star formation rate: this tends to produce a little too much stellar mass at all redshifts. The dotted line provides a much better fit to the build-up of stellar mass, but appears to undershoot somewhat the star formation rate estimates at $z > 1$. The solid line is a reasonable compromise between matching the cosmic star

formation rate and build-up of stellar mass. Despite these interesting tensions at the 30–50 % level — which may indicate deficiencies in stellar mass or SFR estimates (*e.g.* due to a globally incorrect IMF and/or one which varies from galaxy to galaxy), or may betray inappropriate extrapolation to total densities from the observed galaxies — it is nonetheless fair to say that the match between cosmic SFR and the build-up of stellar mass is rather good.

The relatively precise rest-frame colors of COMBO-17 allowed us to separate out the evolution of $\langle \rho_* \rangle(z)$ in red and blue galaxies. While a similar split has not yet been carried out for estimates of cosmic star formation rate, it is interesting to note that study of the UV (Wolf et al. 2005) and UV+IR (Bell et al. 2005a) luminosity of galaxies has demonstrated that the bulk of star formation takes place in spiral galaxies residing in the blue cloud. Thus, one would naively expect that the growth of stellar mass at $z < 1$ would be dominated by a growth in the total stellar mass in blue galaxies. Yet, Fig. 10 shows that the total stellar mass growth takes place mainly in the red sequence. Thus, stars form in blue galaxies, but a substantial fraction of the star-forming galaxy population must globally truncate their star formation and fade and redden onto the red sequence at $z < 1$. A discussion of this point is deferred to a future paper.

6. Summary and Conclusions

We have presented estimates of the stellar masses, derived from SED-fitting of the COMBO-17 flux-points using PEGASE population synthesis models, for 25000 galaxies to $z = 1$, with known redshifts, rest-frame colors and luminosities. From this data set we were able to show the following.

- Since $z \sim 1$ the majority of galaxies with $M > 10^{11} M_\odot$ have been on the red-sequence, *i.e.*, have essentially completed the build-up of their stellar mass.
- As a consequence, the stellar mass function of red and blue galaxies differ strongly from each other at all redshifts from 0 to 1. Red galaxies always dominate the massive end, while blue galaxies dominate the faint end. The mass at which the mass functions cross decreases from $M_* \sim 10^{10.8} M_\odot$ at $z = 1$ to $\sim 10^{10} M_\odot$ at the present day. This evolution in the ‘transition mass’, above which most galaxies are not forming stars, is driven primarily by the increasing prominence of the non-star-forming galaxy population at later times.
- The total stellar mass in galaxies has roughly doubled in the 8 Gyr since $z = 1$. Assuming a Chabrier (2003) IMF, the stellar mass evolution and star formation rate evolution are reasonably consistent: a Kroupa et al. (1993) IMF (which has a stellar M/L for a given SED which is very similar to those of a Chabrier IMF) has a relatively low number of high-mass stars and no consistent interpretation of the cosmic star formation rate and growth of stellar mass can be found.

- Somewhat counter-intuitively, the stellar mass function of blue, star-forming galaxies has stayed more or less constant since $z = 1$; the mass in “dead” red-sequence galaxies has almost tripled over that period. While at $z = 1$ half the stars lived in red sequence galaxies and half in star-forming galaxies, 2/3 of all stars at the present epoch live in red-sequence galaxies.
- Even with 25000 galaxies in three disjoint fields of $30' \times 30'$ each, field-to-field variations limit the precision of $\langle \rho_* \rangle(z)$ estimates to $\sim 30\%$.

There are a number of obvious steps which need to be taken to improve the accuracy and extend the scope of the work presented in this paper. Larger areas, more precise redshifts (particularly spectroscopic), and wider wavelength coverage will give increased precision on the form of the mass function (especially at the high-mass end; critical for exploring the influence of galaxy mergers on the stellar mass function) and increased redshift range. Larger samples of dynamical masses and improved templates will increase the accuracy (*i.e.*, reduce systematic error) in the mass functions. Finally, accurate determinations of star formation rates from Spitzer/Herschel/ALMA will allow star formation and the build-up of stellar mass to be inter-compared at a much more detailed and informative level than is currently possible, further elucidating the role of *in situ* star formation vs. galaxy mergers in driving the mass evolution of the galaxy population.

Acknowledgements. We are grateful to an anonymous referee who made numerous suggestions how to improve this paper. We thank Roelof de Jong and Rachel Somerville for interesting discussions which helped to shape this work, and Michele Cappellari for the data for Fig. 11 in electronic form. E. F. B. was supported by the European Community’s Human Potential Program under contract HPRN-CT-2002-00316 (SISCO).

References

- Adelberger, K. L., & Steidel, C. C. 2000, ApJ, 544, 218
 Baldry, I. K., Galzebrook, K., Brinkmann, J. et al. 2004, ApJ, 600, 681
 Bauer, A. E., Drory, N., Hill, G. J., & Feulner, G. 2005, ApJ, 621, L89
 Bell, E.F., de Jong, R.S., 2001, ApJ 550, 212
 Bell, E.F., McIntosh, D.H., Katz, N., Weinberg, M.D, 2003, ApJS 149, 289
 Bell, E.F., Wolf, C., Meisenheimer, K. et al. 2004, ApJ 608, 752
 Bell, E.F., Papovich, C., Wolf, C. et al. 2005a, ApJ, 625, 23
 Bell, E.F., Naab, T., McIntosh, D. H. et al. 2005b, submitted to ApJ [astro-ph/0506425]
 Bender, R., Burstein, D., & Faber, S. M. 1993, ApJ, 411, 153
 Blumenthal, G. R., Faber, S. M., Primack, J. R., & Rees, M. J. 1984, Nature, 311, 517
 Böhm, A., Ziegler, B. L., Saglia, R. P. et al. 2004, A&A, 420, 97
 Brinchmann, J., & Ellis, R. S. 2000, ApJ, 536, 77L

- Brinchmann, J., Charlot, S., White, S. D. M. et al. 2004, MNRAS, 351, 1151
- Bundy, K., Ellis, R. S., Conselice, C. J. et al. 2006, submitted to ApJ [astro-ph/0512465]
- Calzetti, D., Kinney, A. L., Storchi-Bergmann, T. 1994, ApJ, 429, 582
- Cappellari, M., Bacon, R., Bureau, K. et al. 2005, submitted to MNRAS [astro-ph/0505042]
- Chabrier, G. 2003, ApJ, 586, L133
- Chapman, S. C., Blain, A. W., Ivison, R. J., & Smail, I. R. 2003, Nature, 422, 695
- Cole, S., Aragon-Salamanca, A., Frenk, C. S., Navarro, J. F., Zepf, S. E. 1994, MNRAS, 271, 781
- Cole, S., Lacey, C.G., Baugh, C.M., Frenk, C.S., 2000, MNRAS 391, 168
- Cole, S., Norberg, P., Baugh, C.M. et al., 2001, MNRAS 326, 255
- Conselice, C. J., Bundy, K., Ellis, R. S. et al. 2005, ApJ, in press [astro-ph/0503597]
- Cowie, L. L., Songaila, A., Hu, E. M., & Cohen, J. G. 1996, AJ, 112, 839
- Daddi, E., Dickinson, M., Chary, R. et al. 2005, ApJ, 631, L13
- Davis, M., Efstathiou, G., Frenk, C. S., & White, S. D. M. 1985, ApJ, 292, 371
- Davis, M., Faber, S. M., Newman, J. et al. 2003, in Discoveries and Research Prospects from 6- to 10-Meter-Class Telescopes II. Edited by Guhathakurta & Puragra. Proceedings of the SPIE, Volume 4834, p161.
- de Lucia, G., Poggianti, B. M., Aragón-Salamanca, A. et al. 2004, ApJ, 610, L77
- Dickinson, M., Papovich, C., Ferguson, H. C., & Budavári, T. 2003, ApJ, 587, 25
- Drory, N., Bender, R., Feulner, G. et al. 2004a, ApJ 608, 742
- Drory, N., Bender, R., & Hopp, U., 2004b, ApJ 616, L103
- Drory, N., Salvato, M., Gabasch, A. et al. 2005, ApJ 619, L131
- Fioc, M., Rocca-Volmerange, B., 1997, A&A 326, 950
- Flores, H., Hammer, F., Thuan, T. X. et al. 1999, ApJ, 517, 148
- Fontana, A., Pozetti, L., Donnarumma, I. et al. 2004, A&A, 424, 23
- Giavalisco, M., Dickinson, M., Ferguson, H. C. et al. 2004, ApJ, 600, L103
- Glazebrook, K., Abraham, R. G., McCarthy, P. J. et al. 2004, Nature, 430, 181
- Haarsma, D. B., Partridge, R. B., Windhorst, R. A., & Richards, E. A. 2000, ApJ, 544, 641
- Harris, J., & Zaritsky, D. 2004, AJ, 127, 1531
- Hatziminaoglou, E., Groenewegen, M.A.T., da Costa, L. et al. 2002, A&A, 384, 81
- Heavens, A., Panter, B., Jiminez, R., & Dunlop, J. 2004, Nature, 428, 625
- Hippelein, H., Maier, C., Meisenheimer, K. et al. 2003, A&A, 402, 65
- Holden, B., van der Wel, A., Franx, M. et al. 2005, ApJ, 620, L83
- Hopkins, A. M. 2004, ApJ, 615, 219
- Juneau, S., Glazebrook, K., Crampton, D. et al. 2005, ApJ, 619, L135
- Kauffmann, G. White, S.D.M., Guiderdoni, B., 1993, MNRAS 264, 201
- Kauffmann, G., Heckmann, T.M., White S.D.M. et al. 2003, MNRAS 341, 33
- Kelm, B., Focardi, R. & Sorrentino, G., 2005, A&A 442, 117.
- Kinney, A.L., Calzetti, D., Bohlin, R.C. et al. 1996, ApJ 467, 38
- Kochanek, C. S., Pahre, M. A., Falco, E. E. et al. 2001, ApJ 560, 566
- Kodama, T., Yamada, T., Akiyama, M. et al. 2004, MNRAS, 350, 1005
- Kroupa, P., Tout, C.A., Gilmore, G., 1993 MNRAS 262, 545
- Kroupa, P., 2001 MNRAS 322, 231
- Le Floch, E., Papovich, C., Dole, H. et al. 2005, ApJ, 632, 169
- Lilly, S. J., Tresse, L., Hammer, F., Crampton, D., & Le Fèvre, O., 1996, ApJ, 455, L108
- Lilly, S. J., Le Fèvre, O., Hammer, F., Crampton, D. 1996, ApJ, 460, L1
- Madau, P., Ferguson, H.C., Dickinson, M.E. et al. 1996, MNRAS 283, 1388
- Meurer, G. R., Heckman, T. M., & Calzetti, D. 1999, ApJ, 521, 64
- Murali, C., Katz, N., Hernquist, L., Weinberg, D. H., & Davé, R. 2002, ApJ, 571, 1
- Neri, R., Genzel, R., Ivison, R. J. et al. 2003, ApJ, 597, L113
- Panther, B., Heavens, A. F., & Jiminez, R. 2004, MNRAS, 355, 764
- Papovich, C., Dickinson, M., & Ferguson, H. C. 2001, ApJ, 559, 620
- Rudnick G., Rix H.-W., Franx M. et al. 2003, ApJ 599, 847
- Proctor, R. N., & Sansom, A. E. 2002, MNRAS, 333, 517
- Rocha-Pinto, H. J., Scalo, J., Maciel, W. J., & Flynn, C. 2000, A&A, 358, 869
- Salim, S., Charlot, S., Seibert, M. et al. 2005, ApJ, 619, L39
- Salpeter, E. E. 1955, ApJ, 121, 161
- Saracco, P., Longhetti, M., Severgnini, P. et al. 2005, MNRAS, 357, L40
- Schiminovich, D., Ilbert, O., Arnouts, S. et al. 2005, ApJ, 619, L47
- Springel, V., & Hernquist, L. 2003, MNRAS, 339, 312
- Somerville, R. S., Primack, J. R., Faber, S. M. 2001, MNRAS 320, 504
- Somerville, R. S., Lee, K., Ferguson, H. C. et al. 2004, ApJ, 600, L171
- Steidel, C. C., Adelberger, K. L., Giavalisco, M., Dickinson, M. & Pettini, M. 1999, ApJ, 519, 1
- Tanaka, M., Kodama, T., Arimoto, N. et al. 2005, MNRAS, in press [astro-ph/0506713]
- Thomas, D., Maraston, C., Bender, R., & Mendes de Oliveira, C. 2005, ApJ, 621, 673
- Trager, S. C., Faber, S. M., Worthey, G., & González, J. J. 2000, AJ, 120, 165
- Tremonti, C. A., et al. 2004, ApJ, 613, 898
- van der Wel, A., Franx, M., van Dokkum, P. G., Rix, H.-W., Illingworth, G. D., & Rosati, P. 2005, submitted to ApJ [astro-ph/0502228]
- Vogt, N., Forbes, D. A., Phillips, A. C. et al. 1996, ApJ, 465, L15
- Vogt, N., Phillips, A. C., Faber, S. M. et al. 1997, ApJ, 479, L121
- Wang, B., Heckman, T. M., 1996, ApJ, 457, 645
- Springel, V., & Hernquist, L. 2003, MNRAS, 339, 312
- White, S. D. M., & Rees, M. J. 1978, MNRAS, 183, 341
- Willmer, C. N. A., Faber, S. M., Koo, D. C. et al. 2005, submitted to ApJ [astro-ph/0506041]
- Wolf C., 1999, PhD thesis, Universität Heidelberg
- Wolf, C., Meisenheimer, K., Röser, H.-J., 2001, A&A 365, 660
- Wolf, C., Meisenheimer, K., Rix, H.-W. et al. 2003 A&A 401, 73

- Wolf, C., Meisenheimer, K., Kleinheinrich et al. 2004, A&A
429, 913
- Wolf, C., Bell, E. F., McIntosh, D. H. et al. 2005, ApJ, 630,
771
- Yan, L., McCarthy, P. J., Freudling, W. et al. 1999, ApJ, 519,
L47